Chemistry in Acetone Complexes of Metal Dications: A Remarkable Ethylene Production Pathway

Jianhua Wu, Dan Liu, Jian-Ge Zhou, and Frank Hagelberg*

Computational Center for Molecular Structure and Interactions, Department of Physics, Atmospheric Sciences, and Geoscience, Jackson State University, Jackson, Mississippi 39217

Sung Soo Park

Computer-Aided Engineering Group, Samsung Electro-Mechanic Co. Ltd., Suwon, South Korea

Alexandre A. Shvartsburg

Biological Sciences Division, Pacific Northwest National Laboratory, P.O. Box 999, Richland, Washington 99352

Received: December 13, 2006; In Final Form: March 15, 2007

Electrospray ionization can generate microsolvated multiply charged metal ions for various metals and ligands, allowing exploration of chemistry within such clusters. The finite size of these systems permits comparing experimental results with accurate calculations, creating a natural laboratory to research ion solvation. Mass spectrometry has provided much insight into the stability and dissociation of ligated metal cations. While solvated singly charged ions tend to shrink by ligand evaporation, solvated polycations below a certain size exhibit charge reduction and/or ligand fragmentation due to organometallic reactions. Here we investigate the acetone complexes of representative divalent metals (Ca, Mn, Co, Ni, and Cu), comparing the results of collision-induced dissociation with the predictions of density functional theory. As for other solvated dications, channels involving proton or electron transfer compete with ligand loss and become dominant for smaller complexes. The heterolytic C−C bond cleavage is common, like in DMSO and acetonitrile complexes. Of primary interest is the unanticipated neutral ethylene loss, found for all metals studied except Cu and particularly intense for Ca and Mn. We focus on understanding that process in the context of competing dissociation pathways, as a function of metal identity and number of ligands. According to first-principles modeling, ethylene elimination proceeds along a complex path involving two intermediates. These results suggest that chemistry in microsolvated multiply charged ions may still hold major surprises.

1. Introduction

Complexes of metal ions with organic and biological molecules are a topic that combines problems central to many areas of science. Of interest to physical chemistry is the formation of solvation shells and order in solutions[1] and the structural and phase transitions in finite systems.[2] For inorganic chemistry, the issues are metal coordination in solid-state complexes[3,4] and fundamental organometallic reactivity including the metal catalysis of bond cleavages.[5,6] For biochemistry, ligated metal ions are useful models to understand biological and toxicological processes that involve metal binding,[7−9] for example with respect to hemes and metalloproteins.[7] From the analytical viewpoint, peptides and other organic molecules cationized by metals tend to fragment differently from protonated analogs.[10−13] This often provides more specific or complementary mass-spectrometric identifications, in particular aiding isomer separations[12] and proteomic sequencing strategies.[10,11] The variable yet finite size of microsolvated metal ions makes them an ideal laboratory to develop and validate theoretical methods, such as the geometry optimization algorithms and model potentials needed to describe larger complexes, mesoscopic "droplets", and solutions.[14,15] For smaller complexes, first-principles calculations[16−18] are crucial to interpret and guide experimental work.

The field of microsolvated metal ions has started from singly charged species, which remain the subject of most studies to date. Those complexes are readily produced by many means, including sequential adsorption of vapor molecules on a bare metal cation. Condensation of neutrals on ions is exothermic, and such clusters grow to essentially any size, depending on the vapor temperature and pressure. Ligation of multiply charged metal ions in that manner is prevented by charge reduction. The second and higher ionization energies (IE) of nearly all metals exceed 12 eV (Table 1), while the first IE (IE1) of typical organic molecules range[19] from 8 to 12 eV (9.7 eV for acetone considered here). Hence the transfer of electron from a ligand (L) to metal ion (M) is normally exothermic and occurs on contact, followed by immediate dissociation driven by Coulomb repulsion. Even when the IE1 of L exceeds the second IE (IE2) of M, charge reduction precluding complex formation may still proceed by other routes. For example, an attempt to add water (IE1 = 12.6 eV) to Ca^{2+} results in an interligand H^+ transfer yielding[20] $CaOH^+$ and H_3O^+.

However, polyvalent metal ions are stable in bulk solutions due to charge stabilization by many solvent molecules. Hence

* To whom correspondence should be addressed. E-mail: frank.d.hagelberg@ccaix.jsums.edu.

10.1021/jp068574z CCC: $37.00
Published on Web 05/16/2007

TABLE 1: Summary of Dissociation Properties Measured for $M^{2+}L_n$ (L = Acetone) Complexes

metal	IE2, eV	n_{min}	n_{crit}[a]	C_2H_4 loss[b]	C−C cleavage[d]
Ca	11.9	0	2 (p)	1 (strong)[c]	1 (low)
Mn	15.6	1	3 (p)	2 (strong)	2 (strong)
Co	17.1	1	3 (e, p)	2 (strong)	3 (strong)
Ni	18.2	2	3 (e, p)	2 (low)	2 (significant)
Cu	20.3	3	4 (p)	none	none

[a] Critical size with the pertinent process: (e) electron transfer; (p) H^+ transfer. [b] The *n* for which the reaction occurs, with intensity relative to dominant channel: the dominant channel or same order of magnitude (strong); ~1 order of magnitude less (significant); ~2 orders of magnitude less (low). [c] May be happening for $n = 2$ in a minute yield. [d] Same as footnote *c*, except only the highest *n* for which the reaction occurs is given. The listed intensity is an estimate for all *n* where the process was seen and not just for the highest *n*.

it should be possible to generate microsolvated polycations by desolvation of macroscopic droplets. That process occurs in electrospray ionization (ESI) sources, the advent of which in 1990s had opened such ions to experimental research.[21,22] Those species could also be made by raising the charge state of neutral or singly charged metal centers in complexes large enough to avoid immediate charge transfer between the metal and ligand shell. That could be achieved using laser or electron impact ionization, known respectively as pick-up[3−5,23,24] and charge-stripping[25,26] techniques. These methods may allow metal ion/ligand pairs not amenable to ESI because the ion is unstable even in solution[4] (such as Au^{2+}), the ligand is not a liquid at atmospheric pressure (CO_2),[19,27] or its boiling point is too low (e.g., NO or Ar).[27,28] Also, some complexes not produced by ESI directly could be obtained by ligand exchange in the gas phase.[16,29]

As is obvious from the macroscopic limit, sufficiently large microsolvated ions of any charge state dissociate only by simple ligand loss

$$M^{z+}L_n = M^{z+}L_{n-1} + L \qquad (1)$$

While in some cases that "evaporation" proceeds all the way to bare M^{z+}, for $z > 1$ other channels normally begin appearing at a certain critical size (n_{crit}). Most of those involve charge reduction, and the universal path is the dissociative electron transfer (2) that (in principle) could occur for any ligand and complex size:

$$M^{z+}L_n = M^{(z-1)+}L_{n-k} + (L_k)^+ \qquad (2)$$

This process (with $k = 1$) is common for M^{2+} complexes with aprotic solvents such as acetonitrile,[30−32] dimethyl sulfoxide (DMSO),[33,34] and pyridine;[30,35] $k > 1$ is possible in theory but has not been observed. (A report[36] of $k = 2$ and 3 for $Mn^{2+}(pyridine)_n$ has subsequently been corrected.[27,35]) Ligands with O−H bonds such as water, alcohols, and aldols give off a proton easier than an electron (hence the name "protic solvents"). Instead of (2), their complexes dissociate by interligand H^+ transfer, also followed by Coulomb explosion:

$$M^{z+}L_n = [M(L-H)]^{(z-1)+}L_{n-k-1} + H^+L_k \qquad (3)$$

This has been observed for $k = 2$ or 3 as well as $k = 1$ (depending on L),[37,38] which is not surprising considering that proton-bound clusters of protic molecules are quite stable and ubiquitous in mass spectrometry (MS). This process is also common for complexes with all hydrogen-containing aprotic solvents,[30−35] where it competes with (2). The competition is close overall: the outcome depends on the metal and *n*, with both (2) and (3) seen in many cases. In a series of $M^{2+}L_n$, (2) is generally favored by increasing IE2 of the metal and decreasing *n*. Both trends make sense: e-transfer becomes more exothermic at higher IE2 and a closer distance between ligands at higher *n* facilitates H^+ transfer needed for (3). For basic H-containing ligands such as pyridine,[35] another possible process is interligand hydride transfer, again followed by charge separation:

$$M^{z+}L_n = (MH)^{(z-1)+}L_{n-1} + (L-H)^+ \qquad (4)$$

The hallmarks of the dissociation of microsolvated metal ions with $z > 1$ are ligand breakup channels that, unlike (1)−(4), are obviously ligand-specific. Ligands containing N such as acetonitrile or pyridine are heterolytically cleaved by most M^{2+}, yielding bare or solvated metal cyanides (MCN^+).[32,35] Heterolytic cleavage may also occur for double bonds such as S=O in DMSO,[33] with the metal attaching to either S to form methylsulfides (M^+SCH_3) or O to form (solvated) oxides (M^+O) or hydroxides (MOH^+). Ligands may be cleaved effectively without charge reduction, as shown by sequential elimination[33] of CH_3 radicals from $M^{2+}(DMSO)_n$. Such homolytic cleavages often involve the leaving group abstracting a hydrogen: $M^{2+}(DMSO)_n$ may lose[33] CH_4 and $M^{2+}(pyridine)_n$ lose[35] NH_2, NH_3, or CH_3. The competition between cleavages and reactions (1)−(3) is also largely controlled by the metal IE2. For example, the IE2 of Cu (20.3 eV) is highest of all metals with M^{2+} stable in aqueous media, and Cu^{2+} complexes rarely fragment by ligand cleavage because (2) or (3) has a lower activation barrier.[32,33,35] Another apparent factor is the ion size, making Be^{2+} (the smallest M^{2+}) unusually good at ligand bond scission.[33] Chemical properties of the metal may matter as well. For example, the S=O cleavage in $M^{2+}(DMSO)_n$ is far more prevalent for transition metals with open d-electron shell (Fe, Co, and Ni) than for others (Zn and Cd) with similar IE2 values.[33] That is consistent with the broad expectation for open-shell transition metals to be more reactive toward organic molecules. Such chemical differences are more prominent for triply charged cations that induce a greater diversity of cleavages.[39]

In summary, dissociation of ligated metal polycations involves rich organometallic chemistry. For any ligand, the partition between channels depends on the IE2, size, and chemistry of the metal in ways that could often be rationalized qualitatively as exemplified above. Even when the strongest channels were not intuitive, the overall set of possibilities was predictable, consisting mostly of the severance of any single intraligand bond (with or without H^+ transfer). Some reactions mirrored those known in solution, such as the retro-aldol reaction and dehydration in complexes of M^{2+} with diacetone alcohol.[38]

A key property of microsolvated metal ions is the minimum size (n_{min})—the smallest *n* for which $M^{z+}L_n$ could be produced. Typical n_{min} values for $z = 2$ range[32,33,35] from 0 (when $M^{z+}L_n$ could be desolvated to bare M^{z+}) to 2 or 3, though values as high as 16−17 were reported[40] for $z = 3$.

For M^{2+} complexes,[31,32,34,36,37] typically $n_{crit} < 9$, a size regime accessible to quantum chemical modeling. For instance, ab initio computations at high levels of correlation had predicted the stability of Cu^{2+} ligated by a single H_2O or NH_3 molecule,[41] which stimulated a lively discussion and was eventually verified by experiment.[26,37,42] Modeling of M^{2+} complexes with DMSO, formaldehyde, or acetonitrile[43−45] has demonstrated that stabilities, geometries, and dissociation channels produced by density functional theory (DFT) are also realistic.

Here we use tandem MS and DFT calculations to investigate the dissociation of $M^{2+}L_n$, where L is acetone, for representative metals. Such species and their homologs for other ketones were produced using ESI[7,46] (for Ca, Mg, Zn, and Cu) and the pick-up technique (for Cu, Pb, Mg, Zn, and Ag),[19,27,47−49] but the dissociation chemistry has not been explored in either experiment or theory. We identify the critical and minimum sizes and focus on the fragmentation of $M^{2+}L_n$ with $n_{min} \leq n \leq n_{crit}$. In addition to the standard proton and electron transfer, those complexes exhibit two intense ligand cleavage processes. One is a mundane C−C bond scission similar to that in DMSO complexes.[33] The other is the elimination of neutral ethylene (C_2H_4)—an unforeseen reaction that must involve multiple steps. Understanding this unprecedented behavior is the central point of this work.

2. Experimental Techniques

Measurements were performed using a TSQ 7000 MS/MS instrument (Thermo, San Jose, CA) with ESI source. Samples were pumped to a steel emitter (at ∼4 kV) at a flow rate of several μL/min. We sprayed millimolar solutions of $M(NO_3)_2$ for Ca, Mn, Co, Ni, or Cu in pure acetone. This is similar to the method of Cheng et al.[46] and differs from that of Peschke et al.,[7] who infused methanol solutions and produced $M^{2+}(acetone)_n$ by postionization ligand exchange. Ions produced by ESI were desolvated in a capillary/skimmer cone MS interface. The capillary temperature was varied from 70 to 375 °C to maximize the yield of specific ions, with the optimum depending on the metal and desired n for the precursor. The voltage drop at the skimmer was minimized, creating "mild" ESI conditions conducive to the formation of ligated polycations.[22,46]

Mass-selected precursors were fragmented by collision-induced dissociation (CID) with Ar across the energy range of $E_{lab} = 20-120$ eV (laboratory frame) and the pressure (P) of 1.3 mTorr. This pressure corresponds to multicollisional CID, necessary to induce deep sequential decay of large parent ions on the experimental time scale at reasonable E_{lab}. A similar fragmentation by single collision requires $E_{lab} > \sim 150$ eV, which degrades the mass resolution enough to potentially affect MS assignments. However, some data were verified by measurements at $P = 0.3$ mTorr, which is closer to the single-collision regime.

Interpretation of MS data for ligated metal dications is often complicated by isobaric overlaps. Disentangling these requires isotopic substitutions to the ligand and/or metal. That is a particular challenge for $M^{2+}(acetone)_n$, because of mass coincidences between ^{58}Ni and L (58 Da) and between Co and HL (59 Da) that produce equal m/z for likely ions containing Co or Ni and L in different combinations. To resolve this issue and verify the integrity of assignments in general, whenever possible experiments were repeated with acetone-d_6 and more than one metal isotope.

Another difficulty is created by the covalently bound acetone dimer (diacetone alcohol, DAA)—a common impurity in acetone. Metal cations have a high affinity to DAA, which may result in preferential formation of $M^{2+}(DAA)_n$ complexes.[38] Since $M^{2+}(DAA)_n$ and $M^{2+}L_{2n}$ are isomers, they are not separable in MS using isotopic substitutions. However, CID of $M^{2+}(DAA)_n$ using the same instrument under identical conditions has been characterized for all metals studied here,[38] and new pathways must originate from $M^{2+}L_{2n}$. Also, lack of known fragments of $M^{2+}(DAA)_n$ in a CID spectrum demonstrates that $M^{2+}(DAA)_n$ is not among the parent ions, meaning that all products observed must come from $M^{2+}L_{2n}$.

3. Computational Methods

The geometries for various $M^{2+}L_n$ complexes, observed CID products, and likely intermediates were optimized using hybrid DFT[50] with the B3LYP exchange-correlation functional and 6-311+G** triply split valence basis set. For a number of reactions, transition states (TS) were identified and confirmed by harmonic vibration frequency analysis. To verify that a TS links the reactants and the products of a process, the geometry was deformed along the unstable coordinate in both directions and the resulting structures were relaxed.

The methodology was tested using DFT with a plane wave basis, as implemented in the Vienna ab initio simulation package (VASP).[51−53] Generalized Kohn−Sham equations[54] were solved employing a residual minimization scheme, the direct inversion in the iterative subspace (RMM-DIIS) technique.[55,56] The interaction of valence electrons and core ions was described by the projector-augmented wave (PAW) method[57] within the generalized gradient approximation[58] for the exchange-correlation functional. Periodic boundary conditions were imposed on a cubic 20 Å cell. In the final structures, the smallest distance between atoms in adjacent cells exceeded 10 Å, making the mutual influence of cells negligible. The two procedures produced very close geometries and spin multiplicities in all cases tried.

4. Experimental Findings

Ions of $M^{2+}L_n$ composition were abundant for all metals. Typical distributions comprised $n = 5-8$, often peaking at $n = 6$ (Figure 1a). For Ca, $M^{2+}L_6$ is a "magic" cluster that nearly always dominates the mass spectrum (Figure 1b). Choosing smaller precursors simplifies the CID spectra and allows deeper fragmentation at lower E, so the data were collected for $n = 5$ and/or 6. As $n_{crit} \leq 4$ for all metals studied (below), starting from $M^{2+}L_5$ or $M^{2+}L_6$ permits full elucidation of the dissociation of $M^{2+}L_n$. We will first describe the most diverse chemistry encountered for complexes of metals with intermediate IE2 (∼15−18 eV) and then move to cases of higher and lower IE2 that exhibit subsets of those processes. The key results are summarized in Table 1.

4.1. Overall Picture of $M^{2+}L_n$ Dissociation: Case of Mn. For Mn^{2+} complexes, the smallest $M^{2+}L_n$ obtained from CID (Figure 2) is not bare M^{2+} but $M^{2+}L$ (Figure 2b,c) and $n_{min} = 1$. The largest product other than $Mn^{2+}L_n$ is $[Mn(L_2 - H)]^+$ derived from H^+ transfer (3) and the complementary fragment is H^+L; hence, the precursor was $Mn^{2+}L_3$ and $n_{crit} = 3$ (Figure 2a). Substantial peaks for $\{Mn^+L; L^+\}$ and $\{(MnHL)^+; (L - H)^+\}$ pairs (Figure 2b,c) indicate the electron (2) and H^- (4) transfers appearing in $Mn^{2+}L_2$. It likely also dissociates by (3) yielding $[Mn(L - H)]^+$: while that ion could arise from $[Mn(L_2 - H)]^+$ losing L, high yield of the product relative to the putative parent makes that improbable as a sole pathway. The Mn^+ and MnH^+ species (Figure 2b,c) could come from several sources including Mn^+L and $(MnHL)^+$ evaporating L;

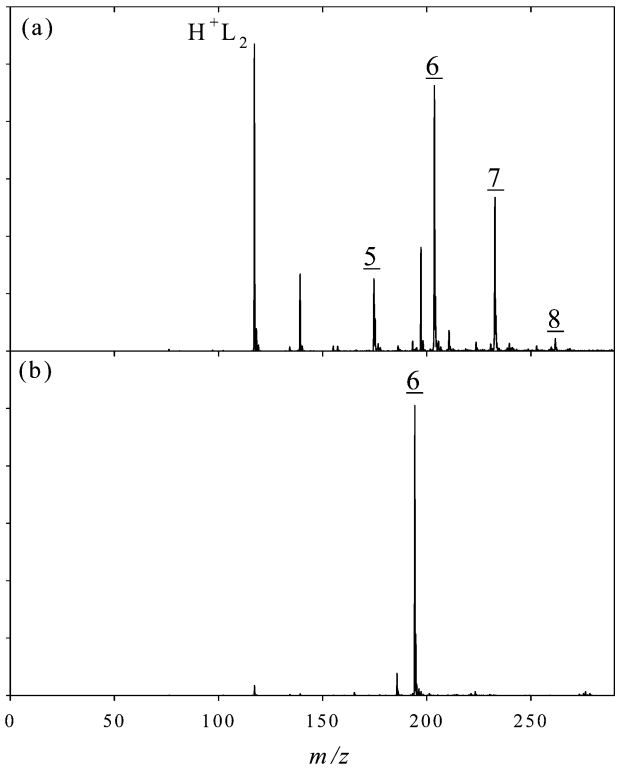

Figure 1. ESI MS spectra for Co^{2+} (a) and Ca^{2+} (b) solutions. Underlined *n* values stand for $M^{2+}L_n$ complexes; L is for acetone.

hence, $Mn^{2+}L$ may undergo either or both processes (2) and (4). These are known behaviors for M^{2+} complexes with aprotic ligands, including the H^+ transfer becoming more competitive to e-transfer at higher *n* (as discussed in the Introduction).

However, $Mn^{2+}L_2$ primarily fragments not by reactions (1)−(4) but by two ligand breakup channels. One is the heterolytic C−C cleavage with the metal attaching to methyl:

$$M^{2+}L_n = M^+CH_3L_{n-1} + CH_3CO^+ \qquad (5)$$

This channel appears for $n = 2$ (no $Mn^+CH_3L_n$ were found for $n > 1$), dominating the dissociation at all sampled *E*. It may also open for $Mn^{2+}L$, but a low signal for this ion prevents clarification whether any of the Mn^+CH_3 fragments come from it rather than Mn^+CH_3L. Reaction (5) resembles the heterolytic C−C cleavage ubiquitous in small $M^{2+}(CH_3CN)_n$, though there the metal attached to cyanide and not methyl.[32] The spectra for ^{1}H-acetone complexes (Figure S1) reveal small $MOHL^+$, MOH^+, and $CH_3CHCH_2^+$ (allyl) features hidden under isobaric peaks in Figure 2. Those are standard products of C═O cleavage in M^{2+}/alcohol complexes, including[38] $M^{2+}(DAA)_n$. Here, they may come from above-mentioned $M^{2+}(DAA)_n$ impurity or may reflect enolization of acetone induced by M^{2+}. Full clarification of this issue is left to future research.

The other cleavage is a hitherto unknown reaction

$$M^{2+}L_n = M^{2+}CH_2O(L)_{n-k-1} + C_2H_4(L)_k \qquad (6)$$

resulting in an intense $Mn^{2+}CH_2OL$ peak (Figure 2b). This was not found for DAA complexes[38] and must come from $M^{2+}L_n$. A neutral leaving group precludes a rigorous determination of *n* in the parent ion, but the absence of $M^{2+}CH_2OL_n$ for $n > 1$ strongly suggests $Mn^{2+}L_2$ ejecting C_2H_4, presumably ethylene. The intensity of $Mn^{2+}CH_2OL$ is somewhat lower than that of M^+CH_3L at all *E* sampled, suggesting that the barrier to process (6) is slightly higher than that to (5). However, the yield of

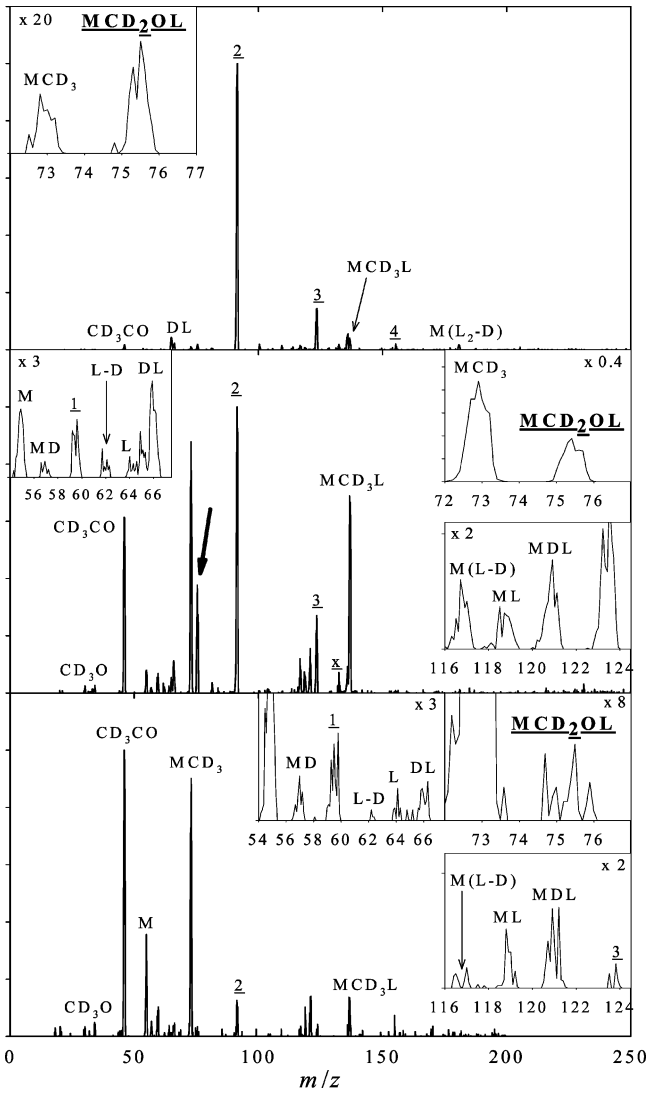

Figure 2. CID spectra for Mn^{2+}(acetone-d_6)$_5$ at $E_{lab} = 40$ eV (a, top), 60 eV (b, middle), and 80 eV (c, bottom). The notation is M for metal, L for acetone, D for deuterium, *n* for $M^{2+}L_n$, and x for fragments[38] of $M^{2+}(DAA)_n$ that could not reasonably come from $M^{2+}L_n$; dications are underlined. Bold font and bold arrows mark the products of (6). Fragments of specific interest are expanded in insets. Assignments are confirmed by spectra for $Mn^{2+}L_5$ (Figure S1).

$Mn^{2+}CH_2OL$ relative to $Mn^{2+}L$ decreases from >20 at $E_{lab} =$ 40 eV (Figure 2a) to ∼5 at 60 eV (Figure 2b) to <1 at 80 eV (Figure 2c). This shows that the barrier to (6) is substantially lower than that to (1), but (1) is kinetically preferred at high energy.

4.2. Complexes of Other Metals with Intermediate IE2: Co and Ni. The pattern for $Co^{2+}L_n$ (Figure 3) broadly resembles that for $Mn^{2+}L_n$. Determination of n_{min} is a challenge because ^{59}Co is the sole stable isotope and $Co^{2+}L$ ($m/z = 58.5$) nearly overlaps with L^+ (58) and Co^+ or H^+L (59). A notable shoulder on a major peak at $m/z = 59$ (Figure S2c,d) emerging at appropriate *E* suggests the presence of $Co^{2+}L$, and acetone-d_6 complexes provide the confirmation (Figure 3c). The $M^+CH_3L_2$ and M^+L_2 features (Figure 3a) indicate the cleavage (5) and e-transfer (2) starting at $n = 3$, in consistency with IE2 of Co exceeding that of Mn (Table 1). The loss of C_2H_4 from $M^{2+}L_2$ is comparable to that for Mn: here (5) is always competitive but clearly preferred at low *E* (Figure 3a), and (2) has a similar intensity at all *E*. The H^+ transfer may also be competitive, which we could not ascertain because $[M(L - H)]^+$ may also come from $[M(L_2 - H)]^+$.

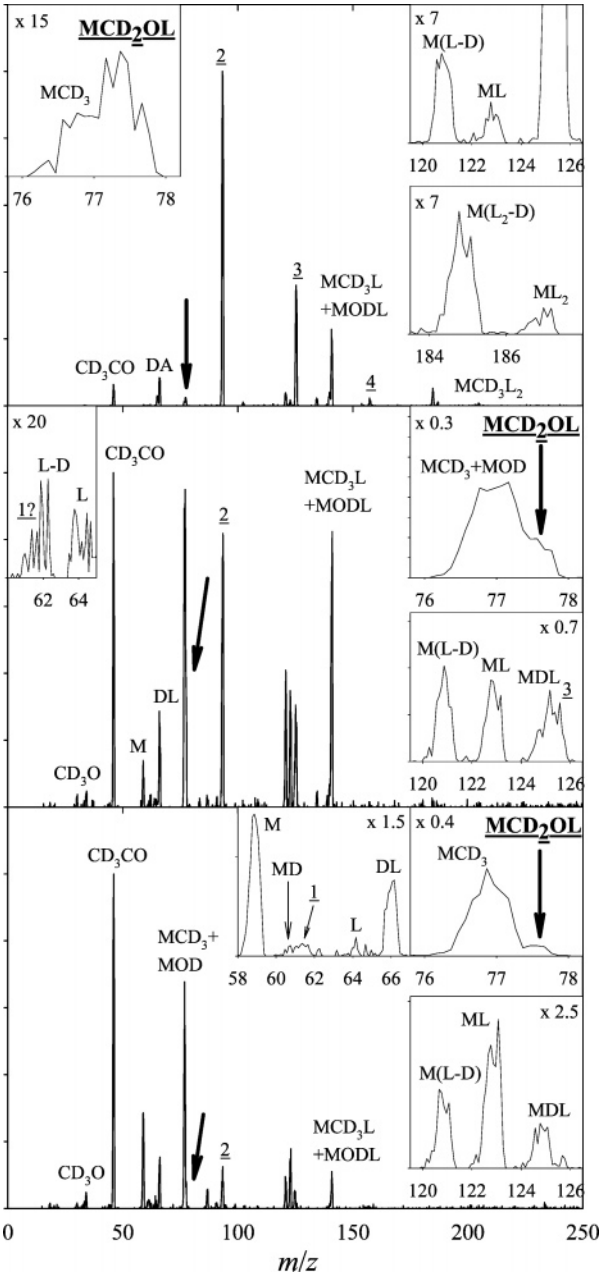

Figure 3. Same as Figure 2 for Co^{2+}(acetone-d_6)$_5$. Assignments are confirmed by spectra for $Co^{2+}L_5$ (Figure S2).

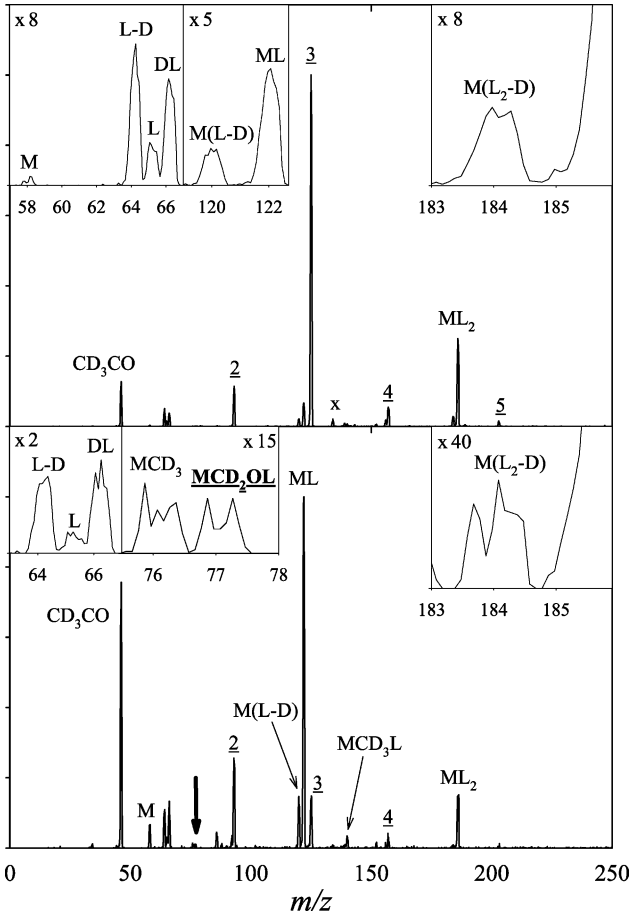

Figure 4. Same as Figure 2 for $^{58}Ni^{2+}$(acetone-d_6)$_6$ at 40 eV (a, top) and 60 eV (b, bottom). Assignments are confirmed by spectra for $^{58}Ni^{2+}L_6$ and $^{60}Ni^{2+}L_6$.

The dissociation of Ni^{2+} complexes (Figure 4) reflects a higher IE2 of Ni compared to Co. Efforts to produce $Ni^{2+}L$ (using acetone-d_6 because of mass coincidences between $^{58}Ni^{2+}L$ and L^+ and between $^{60}Ni^{2+}L$ and H^+L for normal acetone) were unsuccessful, so $n_{min} = 2$. The e-transfer is now strongly favored over H^+ transfer for both $n = 2$ and 3, and H^- transfer is not seen at all. The cleavage (5) is greatly subdued for $n = 1$ and 2 and absent for $n = 3$, and the ethylene loss from $M^{2+}L_2$ is reduced to a trace, the weakest of observed dissociation pathways (Figure 4b).

4.3. Ca and Cu: Metals with Extreme IE2 Values. The lowest IE2 of metals studied is that of Ca. Though it exceeds the IE1 of L by >2 eV, all charge-reducing processes are minor, with H^+ transfer found for $n = 2$ and e-transfer, H^- transfer, and cleavage (5) for $n = 1$ (Figure 5). The weakness of (5) follows the trend of low propensity of alkaline-earth M^{2+} for ligand cleavage.[32,33] Surprisingly, ethylene loss (6) rather than evaporation (1) is the major dissociation pathway of $M^{2+}L$ at all E and may even be the only one as Ca^{2+} could come from $Ca^{2+}CH_2O$. In any event, (6) has a lower barrier than (1) because the ratio of Ca^{2+} and $Ca^{2+}CH_2O$ intensities increases at higher E. Dissociation of $Ca^{2+}L_2$ is dominated by (1), with unconfirmed traces of $Ca^{2+}CH_2OL$ hinting at (6) proceeding in a minute yield.

At the other extreme, Cu has the highest IE2 of all normally divalent metals. As for other ligands,[32,33] this results in totally different dissociation properties (Figure 6). The H^+ transfer starts at $n_{crit} = 4$ (Figure 6a), but e-transfer is the dominant or only channel for $n = 3$, as the small $Cu^+(L_2 - H)$ peak could come from $Cu^+(L_3 - H)$. In any case, $Cu^{2+}L_2$ could not be found and $n_{min} = 3$. Neither cleavage (5) nor ethylene loss were found for any n, hardly surprising given that both processes appear to occur for $n \leq 2$ only (save for a tiny yield of (5) in the case of Co).

4.4. Summary of Experimental Results. The minimum and critical sizes for M^{2+}/acetone combination are respectively 0−3 and 2−4, increasing as the metal IE2 shifts from 12 to 20 eV. Below n_{crit}, the dissociation involves various charge-reducing pathways: the electron transfer; interligand H^+ and H^- transfers; C−C cleavage. The competition between those channels is largely governed by the metal IE2. Those patterns follow the trends found for M^{2+} ligated by other aprotic solvents such as acetonitrile and DMSO.[32,33] New and distinct here is the elimination of neutral C_2H_4 from M^{2+}(acetone)$_n$ with $n = 1$ or 2, which must involve a complete ligand rearrangement with severance of two covalent (C−C and C═O) and two C−H bonds. The observed intensity of this process for complexes of most metals, competitive with or winning over the breaking of a van der Waals M^{2+}−acetone interaction for ligand evaporation, one C−H bond for H^+ or H^- transfer, or a single C−C

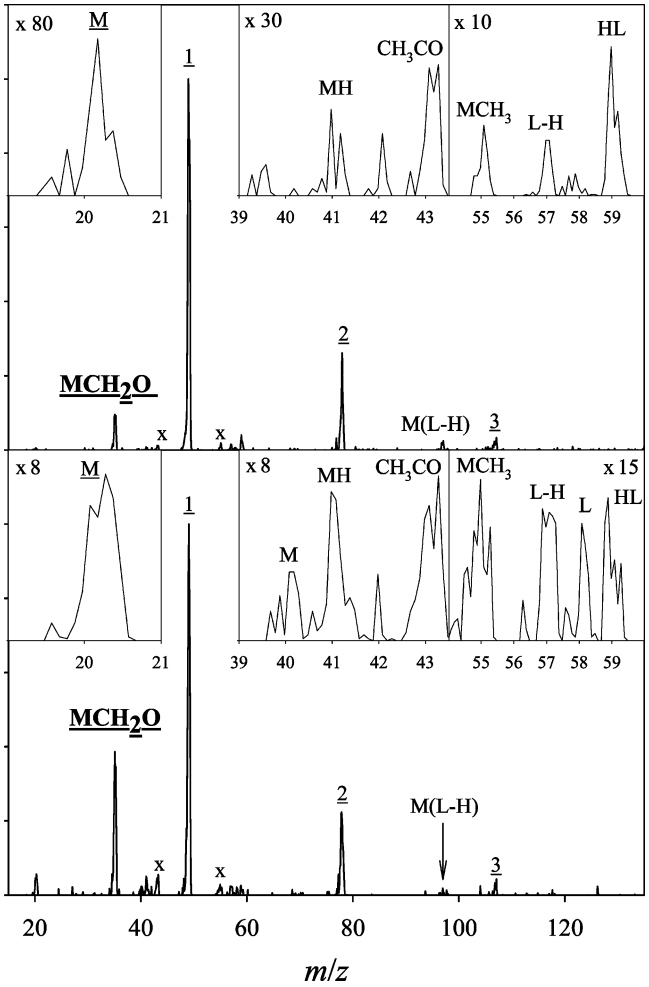

Figure 5. Same as Figure 2 for $^{40}Ca^{2+}L_5$ at 60 eV (a, top) and 80 eV (b, bottom).

bond, is highly surprising. We will now try to understand this behavior using first-principles calculations.

5. Computational Results

We have modeled the structures and dissociation pathways for complexes of all five metals studied in present experiments. The choice of processes to investigate was informed by measurements, but some other plausible channels were also considered. Thorough fragmentation modeling was limited to $M^{2+}L$ and $M^{2+}L_2$ precursors for computational constraints and because most chemistry of interest occurs for $n \leq 2$ (section 4). However, ligand evaporation was considered for $n = 3-5$. Both dissociation energies (D) and activation barriers (E) were calculated in most cases, with all quantities expressed in eV and summarized in Table 2. We first describe the mechanisms and energies of specific pathways and then synoptically compare them with experiment.

5.1. Geometries of M^{2+}(acetone)$_n$ Complexes. To gauge the geometries of $M^{2+}L_n$ precursors to the reactions studied here, we have optimized $Ca^{2+}L_n$ and $Mn^{2+}L_n$ for $n = 1-5$. All ligands are in the first solvation shell, with O atoms coordinated to the metal. As usual, ligands seek maximum separation from each other (Figure 7), and the length of the M−O bond (d_{M-O}) increases with n because the metal−ligand interaction weakens as the number of ligands grows. For example, a tetrahedron (S_4) for $n = 4$ and deformed bipyramid (D_{3h}) for $n = 5$ are stable while planar structures have an imaginary frequency for

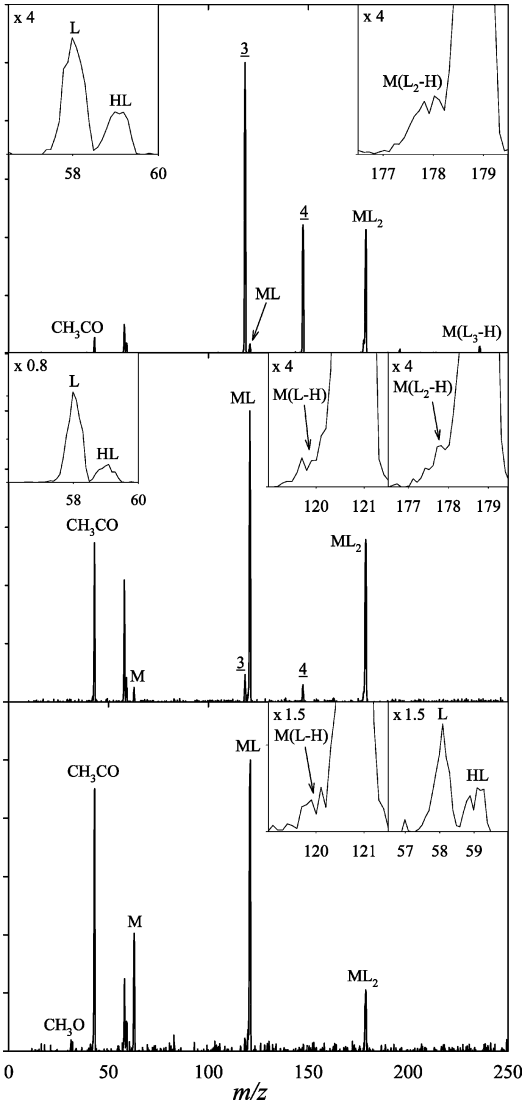

Figure 6. CID spectra for $^{63}Cu^{2+}L_5$ at $E_{1ab} = 20$ eV (top), 40 eV (middle), and 60 eV (bottom). Assignments are confirmed by spectra for $^{63}Cu^{2+}$(acetone-d_6)$_5$ and $^{65}Cu^{2+}L_6$.

both n. In $Ca^{2+}L_n$, $d_{Ca-O} = 2.08$ ($n = 1$), 2.16 (2), 2.21 (3), 2.26 (4), and 2.32 Å (5).

5.2. Charge-Conserving Dissociation Pathways.

5.2.1. Acetone Evaporation (1). Since the reverse process (ligand condensation on ions) has no energy barrier, $E(1)$ should equal $D(1)$. As is known for metal ion complexes with acetone or other ligands[7,16] and indicated here by M−O bond lengthening, $D(1)$ rapidly increases for decreasing n, from ∼1.7 eV for $n = 4$ to ∼4.0−8.5 eV for $n = 1$ (Table 2). For $n = 1$, $D(1)$ strongly depends on the metal IE2, rising from ∼4.0 eV for Ca to ∼8.5 eV for Cu. This trend greatly weakens for $n = 2$ and disappears for $n > 2$: all $D(1)$ values are ∼2.4 eV for $n = 3$ and (except for M = Ca) ∼4.0−4.3 eV for $n = 2$ (Table 2). This will be of crucial significance for the dissociation pattern.

5.2.2. Ethylene Elimination (6). A highly nonintuitive finding of present experiments is the effective elimination of C_2H_4 from some $M^{2+}L_n$ ($Mn^{2+}L_2$, $Co^{2+}L_2$, and $Ca^{2+}L$). Calculations show that to be a complex process involving two TS and two intermediates, for either $n = 2$ or 1.

For $M^{2+}L_2$ precursors, the O−M−O angle is 180° and ligand planes are mutually perpendicular (Figure 8). In step I, one acetone turns into propanal with a hydrogen atom H(6) transferring from C(5) to C(3). This rearrangement is driven

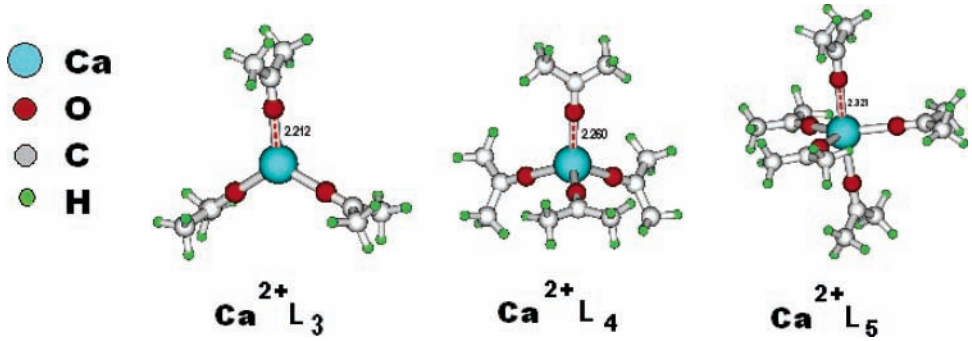

Figure 7. Calculated geometries of $Ca^{2+}L_n$ with $n = 3-5$.

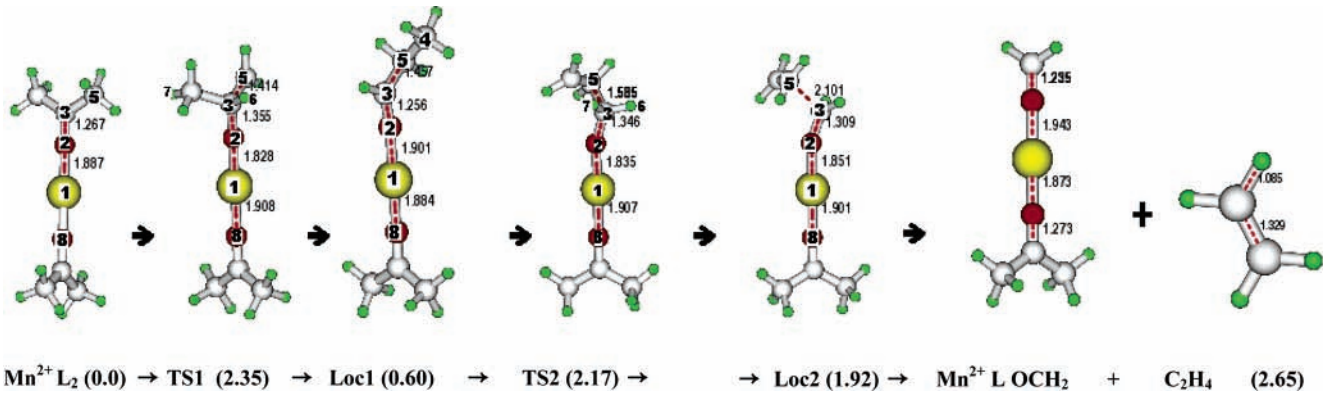

Figure 8. Ethylene elimination from $Mn^{2+}L_2$: stationary point geometries and their energies.

TABLE 2: Calculated Energy Barriers to Processes (1−3, 5, 6) for $M^{2+}L_n$ Species Studied in This Work[a]

		element (IE2, eV)				
channel	*n*	Ca (11.9)	Mn (15.6)	Co (17.1)	Ni (18.2)	Cu (20.3)
1	1	3.99	5.56	6.65	7.15	8.48
	2	2.97	4.02	4.28	4.34	4.05
	3	2.36	2.47	2.48	2.45	2.34
	4	1.76	1.68	1.71	1.68	1.73
2	1	2.86	1.76	1.11	0.76	0.07
	2	>2.69[b]	2.55	2.17	1.73	1.08
3	2	3.27	3.21	2.86	2.68	2.39
5	2	3.75	2.86	2.55	2.45	2.27
6	1	2.68	3.05	3.21	3.33	3.55
	2	2.65	2.65	2.77	2.72	2.72

[a] The branching of dissociation pathways with energies for relevant secondary reactions is exemplified for Mn complexes (Figure S3). [b] The TS has not been identified; $D = 2.69$ eV provides the lower limit for E.

by a structural resonance involving the linear segment O(8)−Mn(1)−O(2)−C(3). One of the resonance structures contains a radical-like C(3) with O(2)−C(3) bond elongated from 1.267 Å in the reactant to 1.355 Å in TS1. In that geometry, H(6) transfers from C(5) to C(3) via the C(3)−C(5)−H(6) ring. For Mn, the barrier to that reaction is 2.35 eV. This strengthens and shortens the O(2)−C(3) bond, and the adjacent methyl $C(4)H_3$ moves from C(3) to C(5) forming intermediate 1.

In step II, there is a similar hydrogen transfer between two carbon centers (Figure 8). The O(2)−C(3) bond elongates and weakens again in TS2, and H(7) transfers from C(4) to C(3) via the C(3)−C(5)−C(4)−H(7) ring. For Mn, the barrier to that reaction is 1.57 eV. This barrier is lower than that in step I because the four-member ring is less strained than the three-member ring in step I. The severance of C(3)−C(5) bond leads to intermediate 2—a noncovalent complex of M^{2+}(acetone)(formaldehyde) with ethylene. The final dissociation involves no TS: the energy rises upon removal of C_2H_4 until the dissociation asymptote is reached. For Co, $E > D$, and the reaction kinetics is controlled by TS1.

The path of ethylene elimination from $M^{2+}L_2$ for other metals is similar. As seen in Figure 8, the other ligand is just a spectator and, hence, the same mechanism works for $M^{2+}L$ such as $Ca^{2+}L$ (Figure 9). Here TS1 is also higher than TS2 but somewhat lower than the dissociation asymptote and $E = D$. The energies of species involved in the process (6) for $Ca^{2+}L$, $Mn^{2+}L_2$, and $Co^{2+}L_2$ are placed in the context of competing channels in Figure 10a−c. Importantly, $E(6)$ for bisligand precursors is ∼2.7 eV with all five metals (Table 2).

5.2.3. Methyl Radical Loss. For $M^{2+}(DMSO)_n$ complexes of most divalent metals including Ca, Mn, and Co,[33] elimination of CH_3 upon C−S bond cleavage is a dominant or major pathway, especially for $n = 2$. The acetone molecule differs from DMSO only by C replacing S, and one might expect the reaction 7 to be common for M^{2+}/acetone complexes:

$$M^{2+}L_n = M^{2+}CH_3COL_{n-1} + CH_3 \qquad (7)$$

However, no $M^{2+}CH_3COL_{n-1}$ product was detected for any $M^{2+}L_n$ precursor. For all five metals, calculated $D(7)$ for $n = 1$

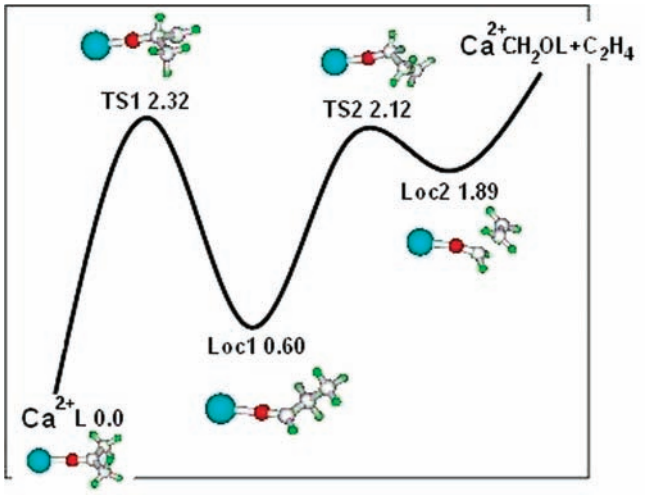

Figure 9. Same as Figure 8 for $Ca^{2+}L$.

and 2 exceeds ~3.9 eV (Figure 10a−c). That is higher than E for (6) and other channels (below) by >1.0 eV. This explains why (7) is not seen in present experiments, and we will not consider it further. In contrast, modeling of $Sc^{3+}(DMSO)_n$ dissociation using similar methods[16] has found the CH_3 loss to be competitive, in agreement with measurements.[39] This difference mainly reflects that a C−C bond is much stronger than a C−S bond.

5.3. Charge-Reducing Pathways. As ligated polycations shrink, Coulomb repulsion of charges increasingly favors charge-reducing fragmentation pathways. The most elementary of those is the ligand-to-metal e-transfer followed by L^+ loss (2) and interligand H^+ transfer with subsequent separation of $[M(L-H)]^+L_{n-2}$ and H^+L (3). Both were observed in present experiments, along with elimination of CH_3CO^+ consequent upon C−C bond cleavage (5). We now consider these pathways in detail.

5.3.1. Electron Transfer (2). The energy gained by (2) is [(metal IE2) − (ligand IE1)]; thus, a higher IE2 increases the gain and favors this reaction. This trend is general to ligated metal polycations,[16,17,59] and acetone complexes are no exception: $E(2)$ is strongly anticorrelated with the metal IE2, decreasing on the way from Ca to Cu from >2.69 to 1.08 eV for $n = 2$ and from 2.86 to 0.07 eV for $n = 1$ (Table 2). Because of stronger electronic screening of the metal ion by a greater number of ligands, $E(2)$ for any metal increases with higher n.

5.3.2. H^+ Transfer (3). This reaction may start from the metal binding to a methyl C of one acetone (forming the M−O−C−C ring), which brings an adjacent H atom sufficiently close to the O of another acetone for H^+ to jump between the ligands. This is a one-step process for either $n = 2$ (Figure 11a) or $n = 3$ (Figure 11b): instead of relaxing into $[M(L - H)(L + H)]^{2+}L_{n-2}$ intermediate, the TS leads directly to products. In the $[M(L - H)]^+L_{n-2}$ fragment, (L − H) is bound to M at both C of the CH_2 and O (Figure 12). As expected for charge-reducing processes, the values of $E(3)$ decrease with increasing metal IE2 (Table 2). However, the drop is less rapid than that for (2), e.g., by 0.9 vs >1.6 eV from $Ca^{2+}L_2$ to $Cu^{2+}L_2$. Thus, a higher IE2 progressively favors e-transfer over H^+ transfer, with $[E(3) - E(2)]$ increasing from <0.6 eV for $Ca^{2+}L_2$ to >1.3 eV for $Cu^{2+}L_2$.

The computed $E(3)$ for $Co^{2+}L_3$ (Figure 11b) is 2.42 eV—below that for $Co^{2+}L_2$ by ~0.4 eV, confirming the expectation for $E(3)$ to decrease with increasing n (section 1). This trend makes (3) more competitive with (2) for larger n; e.g., $E(3)$ essentially equals $E(2)$ for $Co^{2+}L_3$.

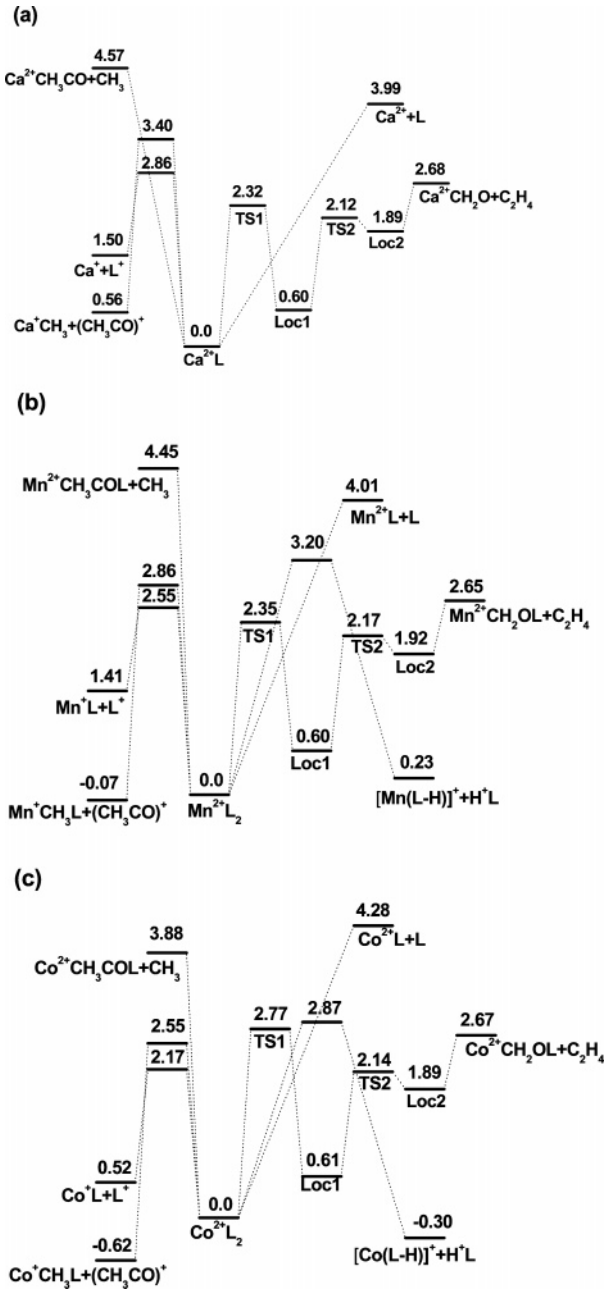

Figure 10. Major dissociation channels and their energies for $Ca^{2+}L$ (a), $Mn^{2+}L_2$ (b), and $Co^{2+}L_2$ (c).

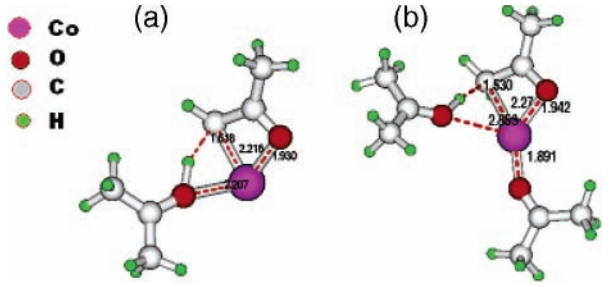

Figure 11. Transition states for interligand H^+ transfer in $Co^{2+}L_2$ (a) and $Co^{2+}L_3$ (b).

5.3.3. CH_3CO^+ Elimination (5). This reaction belongs to the class of heterolytic C−C cleavages that are common to dissociation of M^{2+} complexes with organic ligands. Unlike acetamide complexes where two TS are involved,[59] here (5) may proceed via a single TS. The first step is the same as that for H^+ transfer (eq 3): the metal binds to a methyl C of one

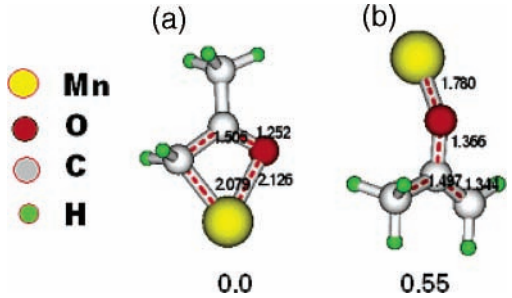

Figure 12. Possible isomers for the $[Mn(L - H)]^+$ product of interligand H^+ transfer in $Mn^{2+}L_2$ and their relative energies. The ring structure (a) is more stable than the open alternative (b).

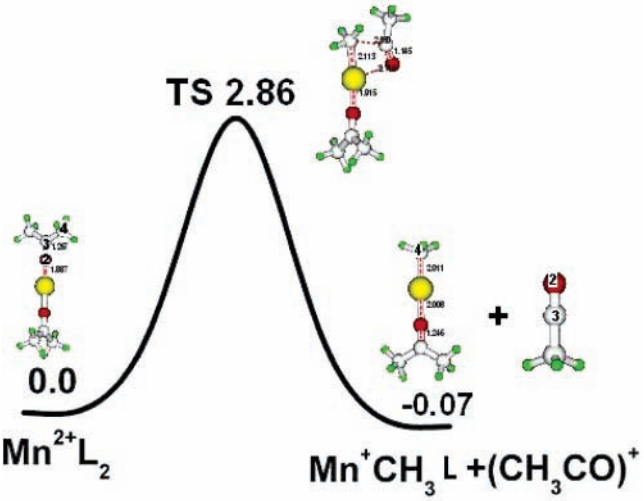

Figure 13. Pathway for the elimination of CH_3CO^+ from $Mn^{2+}L_2$.

acetone making the M−O−C−C ring (Figure 13). In this case, no other ligands get involved. In the TS, the O(2)−C(3) bond contracts while Mn−O(2) and C(3)−C(4) bonds elongate from 1.89 to 2.72 Å and from 1.48 to 2.35 Å, respectively, forming a weakly interacting $Mn^+CH_3L_{n-1}{\cdot}CH_3CO^+$ complex. Then the two weakened bonds are severed and $Mn^+CH_3L_{n-1}$ and CH_3CO^+ separate. $E(5)$ decreases at higher IE2 (Table 2), again as is common for charge-reducing processes. Interestingly, this pathway yields lowest energy products for both $M^{2+}L_2$ and $M^{2+}L$ (Figure 10).

6. Comparison between Modeling and Experiment

6.1. Ethylene Elimination. Again, our most remarkable experimental finding is abundant ethylene loss (6) from many $M^{2+}L_n$. Modeling supports a nonintuitive fact that the barriers to (6) may be very competitive with those for the expected simple processes. For $Mn^{2+}L_2$ with highest yield of (6) among all $M^{2+}L_2$ studied, computed $E(6)$ is virtually equal to E for e-transfer (2) and lower than those for other pathways (Table 2). As the metal IE2 increases, $E(6)$ does not change but (6) becomes less favored because $E(2)$ decreases: for $M^{2+}L_2$ in the Mn−Co−Ni sequence, $[E(6) - E(2)]$ equals 0.1, 0.6, and 1.0 eV, respectively. The pathway (6) also loses to CH_3CO^+ elimination (5), with $[E(6) - E(5)]$ equal to −0.21, 0.22, and 0.27 eV, respectively. The measurements reflect these trends: (6) reduces from a major channel for M = Mn and Co to a trace for Ni (Figures 2−4, 6). Both computed trends extend to $Cu^{2+}L_2$, though this is irrelevant as that species is not produced (below) and the issue of its dissociation is moot.

Simulations also tell why (6) does not occur for $n > 2$. A value of ∼2.2−2.6 eV could be projected for $E(6)$ at $n = 3$ (for all M) by extrapolation from $n = 1$ and 2. This is comparable to $E = 2.34-2.48$ eV for acetone evaporation (1) from $M^{2+}L_3$ (Table 2), but considering the complexity of (6) compared to (1) and the nature of transition states involved [presumably a tight TS for (6) vs a loose/orbiting TS for (1)],[60] (1) should be greatly favored over (6) at equal E by the preexponential factor. One could also estimate $E(2)$ for $n = 3$ using the values for $n = 1$ and 2 and considering that the difference between $E(2)$ for $n = 3$ and 2 must be less than that between $n = 2$ and 1. This yields $E(2) < 2.1$ eV for $Cu^{2+}L_3$, which then should dissociate via (2) rather than (1) or (6). Exactly that is observed in experiment, with $n_{min} = 3$ for Cu (Table 1). The H^+ transfer (3) may also win over (6) for $n = 3$: while $E(3)$ for $Co^{2+}L_3$ (section 5.3.2) is close to the estimated $E(6)$, the pathway (3) involving just one TS is perhaps favored over (6) by kinetics. Refinement of these comparisons using actual rather than estimated $E(2)$ and $E(6)$ for $n = 3$ is left to future work. Decrease of $E(1)$ to ∼1.7 eV for $n = 4$ excludes any possibility of (6) for $n > 3$. In the other limit, the lack of (6) for $Mn^{2+}L$ and $Co^{2+}L$ is due to $E(2)$ being lower than $E(6)$ by ∼1.3 and 2.1 eV (Table 2), while $Ni^{2+}L$ is not even produced.

The agreement between modeling and measurements is worse for Ca complexes. For $n = 2$, the channel (6) is lower than (1) by 0.3 eV, yet in experiment (1) dominates (Figure 5). This may be due to kinetics favoring (1) over (6) as stated above. For $n = 1$, calculations show (6) to be the lowest pathway by 0.2 eV, and (6) is the major channel in experiment.

The modeling overall meshes well with the observation of prominent ethylene elimination (6) from M^{2+}/acetone complexes, though not every detail is reproduced. The process is weaker than calculations suggest for some precursors, including $Ca^{2+}L_2$ mentioned above and $Mn^{2+}L_2$ where (6) appears weaker than (5) (section 4.1) despite computed $E(5)$ exceeding $E(6)$ by 0.2 eV. Quantitative assessment of experimental yields requires incorporating kinetic factors that depend on the nature of transition state(s). These considerations likely favor any of the reactions (1)−(5) that involve (at most) one TS over a two-TS process (6). It is all the more notable that ethylene loss is such a competitive dissociation channel.

6.2. Ligand Evaporation vs Other Reactions. Calculations give further insight into other dissociation properties of M^{2+}/acetone complexes. One is the usual increase of n_{min} and n_{crit} at higher metal IE2 (Table 1). Unfortunately, these parameters are not directly related to E values. By definition, n_{min} is the largest n for which the ligand evaporation (1) is weak enough to be absent in the recorded spectra. Setting kinetic factors aside, that happens when $E(1)$ is much higher than E for at least one other channel. However, the needed gap is hard to quantify because the branching ratio between any two channels depends on the precursor energy that is not defined in multicollisional dissociation. Even in the single-collision regime, this "weak enough" criterion depends on instrumental sensitivity and dynamic range that vary between different MS systems by orders of magnitude and on the chemical noise level that is controlled by sample and source conditions. The situation is similar for n_{crit}—the smallest n for which any process besides (1) is weak enough to not be seen in experiment, such that E for all other channels is much higher than $E(1)$. Hence one should view measured n_{min} and n_{crit} as respectively higher and lower limits of the true values. Successive measurements using better instrumentation or methods have often decreased n_{min} and raised n_{crit}, as evidenced by the work[37,61,62] on hydrated Cu^{2+} and other M^{2+}.

Hence relating the measured n_{min} or n_{crit} to theory quantitatively requires single-collision experiments as a function of ion

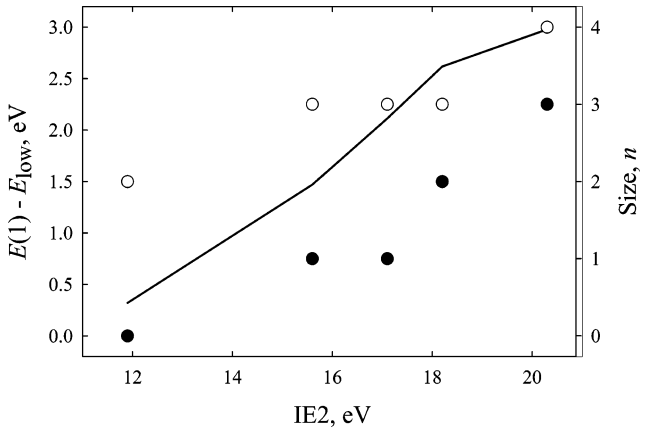

Figure 14. Relative barrier to acetone evaporation (1) in $M^{2+}L_2$ (line, left axis) in comparison with measured characteristic sizes of $M^{2+}L_n$ complexes (filled symbols for n_{min} and empty symbols for n_{crit}, right axis).

energy (such as performed in guided-ion beam tandem MS systems at low gas pressure)[63] and detailed calculations of energy-dependent branching ratios between different pathways that account for kinetics. However, a qualitative comparison could be made on the basis of the present data, using the quantity $[E(1) - E_{low}]$ (where E_{low} is the lowest E) that conveys the energetic propensity of a particular complex to dissociate by pathways other than ligand evaporation. The trends of both n_{min} and n_{crit} for all five metals track the calculated values of $[E(1) - E_{low}]$ for $n = 2$ (Figure 14), which broadly demonstrates the merits of present modeling.

6.3. Charge-Reducing Processes. Calculations provide correct trends for competition between e-transfer (2) and H^+ transfer (3) in $M^{2+}L_n$ as a function of both M and n. As stated in section 5.3.2, $[E(3) - E(2)]$ for $n = 2$ increases in the sequence Ca−Mn−Co−Ni−Cu from <0.6 to 0.66 to 0.69 to 1.0 to 1.3 eV. This trend is in agreement with the measured fragmentation of $M^{2+}L_2$, where the yield of (2) relative to (3) shifts from 0 for Ca (Figure 5) to ∼1 for Mn and Co (Figures 2, 3) to >2 for Ni (Figure 4) to >10 for Cu (Figure 6). The apparently high yield of (3) for M = Co and Mn despite $E(2)$ lying by ∼0.7 eV lower seems like a discrepancy between theory and experiment, especially as the intensity of (3) relative to (2) increases at lower E_{lab} (Figures 2−4) implying $E(3) < E(2)$. However, some $[M(L - H)]^+$ fragments, particularly at lower E_{lab}, likely result not from $M^{2+}L_2$ via (3) but from $[M(L - H)]^+L$ [produced via (3) for $n = 3$] losing L. This removes the disagreement between calculations and measurements for competition between (2) and (3) for $n = 2$.

The major decrease of calculated $[E(3) - E(2)]$ between $n = 2$ and 3 (section 5.3.2) matches the observed shift of branching between H^+- and e-transfers toward the first for all M where either occurs at $n = 3$ (Figures 2−4, 6). At the low end of the IE2 range where (3) is already effective for $n = 2$, the shift is complete with no (2) found for $Mn^{2+}L_3$ (Figure 2). The effect of metal IE2 on the competition between (2) and (3) described above for $n = 2$ also applies for $n = 3$, where the branching ratio between (2) and (3) rises with increasing IE2 from 0 for Mn to >10 for Cu.

Finally, our modeling matches the trend of propensity for C−C cleavage (5) depending on the metal. The calculated values of $[E(5) - E_{low}]$ for $n = 2$ in the Ca−Mn−Co−Ni−Cu sequence are 1.10, 0.31, 0.38, 0.72, and 1.19 eV (Table 2). This progression is consistent with observed yields of (5), characterized respectively as low, strong, strong, significant, and none (Table 1). Again, possible secondary fragmentations should be considered carefully. For example, a prominent CH_3CO^+ product suggests an intense process (5) for $Cu^{2+}L_n$ (Figure 6), but the absence of complementary $Cu^+CH_3L_{n-1}$ for any n disproves that. Instead, CH_3CO^+ likely comes from L^+ produced by dominant channel (2), which by calculations requires just 1.1 eV (Figure S3).

In this context, a fundamental methodological problem of measuring charge-reduction processes for multiply charged ions is large kinetic energy release resulting from Coulomb repulsion of separating ionic products. Even in true threshold dissociation, this could readily cause further CID of one or both fragments potentially preventing their observation and identification. For example, H^+ transfer (3) for $n = 2$ and CH_3CO^+ loss (5) for $n = 1$ and 2 produce 2.9−3.2 eV (Figure 10) of kinetic energy, or >1.4 eV for the lighter fragment that carries most of the energy release. This exceeds the barrier to dissociation of some fragments such as L^+ given above, substantiating the feasibility of their strong attenuation in CID spectra.

7. Conclusions

The dissociation pathways of metal dication−acetone complexes of the form $M^{2+}L_n$, with $n \leq 6$ and M = Ca, Mn, Co, Ni, and Cu, have been investigated by tandem MS. Like other multiply charged ligated metal cations, these species shrink by ligand evaporation until a critical size is reached, rising from 2 to 4 as the metal second ionization energy (IE2) increases in the above sequence. Below that size, there are three types of behavior. For M = Ca with low IE2 (12 eV), fragmentation is dominated by elimination of neutral ethylene. For M = Ni and Cu with high IE2 (>18 eV), prevailing pathways involve charge reduction and the major is the loss of L^+ upon electron transfer to the metal. For M = Mn and Co with intermediate IE2 (15−17 eV), complex fragmentation patterns reflect charge-conserving ethylene elimination coexisting with charge-reducing channels that include e-transfer, loss of H^+L upon interligand H^+ transfer, loss of $(L - H)^+$ upon H^- transfer, and ejection of CH_3CO^+ severed from acetone. While these and other channels involving simple bond cleavages and/or electron jumps were seen in M^{2+} and M^{3+} complexes with various ligands, nothing like ethylene elimination that requires a complete ligand rearrangement has previously been found for miscrosolvated ions.

Activation barriers to the observed and some other conceivable pathways have been modeled using DFT at the B3LYP/6-311+G** level. Though not all details are reproduced, the overall agreement between computed and measured behaviors is quite good. In particular, theory adequately describes the trends of minimum and critical complex sizes, the competition between proton and electron transfer as a function of metal and number of ligands, and the propensity for C−C cleavage depending on the metal. Most importantly, calculations identify the likely mechanism of ethylene loss involving a complicated path with two transition states and show that it indeed is a thermochemically competitive dissociation pathway for complexes of metals with low-to-intermediate IE2. This process has not been considered prior to experimental observation. A continued exploration of chemistry in microsolvated ions may well reveal further surprises of this nature.

Acknowledgment. This work was supported by NSF Grants HRD-9805465 and DMR-0304036, NIH Grant S06-GM008047, the AHPCRC under Cooperative Agreement No. DAAD 19-01-2-0014, the DoD through the U.S. Army/Engineer Research

and Development Center (Vicksburg, MS), Contract No. W912HZ-06-C-0057, and the DoE OBER. We are grateful for insightful discussions with Professor K. W. M. Siu (York University, Toronto, Canada) who has kindly shared his data prior to publication.

Supporting Information Available: CID spectra for $Mn^{2+}L_5$ and $Co^{2+}L_5$ at various energies, further a schematic representation of dissociation pathways for $Mn^{2+}L_n$ with energies for some relevant secondary reactions.This material is available free of charge via the Internet at http://pubs.acs.org.

References and Notes

(1) Berces, A.; Nukada, T.; Margl, P.; Ziegler, T. *J. Phys. Chem. A* **1999**, *103*, 9693.
(2) Rodriguez-Cruz, S. E.; Jockusch, R. A.; Williams, E. R. *J. Am. Chem. Soc.* **1999**, *121*, 1986.
(3) Puskar, L.; Tomlins, K; Duncombe, B.; Cox, H.; Stace, A. J. *J. Am. Chem. Soc*. **2005**, *127*, 7559.
(4) Walker, N. R.; Wright, R. R.; Barran, P. E.; Murrell, J. N.; Stace, A. J. *J. Am. Chem. Soc*. **2001**, *123*, 4223.
(5) Walker, N. R.; Wright, R. R.; Barran, P. E.; Stace, A. J. *Organometallics* **1999**, *18*, 3569.
(6) O'Hair, R. A. J.; Vrkic, A. K.; James, P. F. *J. Am. Chem. Soc*. **2004**, *126*, 12173.
(7) Peschke, M.; Blades, A. T.; Kebarle, P. *J. Am. Chem. Soc.* **2000**, *122*, 10440.
(8) Mazzuca, D.; Russo, N.; Toscano, M.; Grand, A. *J. Phys. Chem. B* **2006**, *110*, 8815.
(9) Rezabal, E.; Mercero, J. M.; Lopez, X.; Ugalde, J. M. *J. Inorg. Biochem.* **2006**, *100*, 374.
(10) Gatlin, C. R.; Rao, R. D.; Turecek, F.; Vaisar, T. *Anal. Chem*. **1996**, *68*, 263.
(11) Chu, I. K.; Guo, X.; Lau, T. C.; Siu, K. W. M. *Anal. Chem.* **1999**, *71*, 2364.
(12) Satterfield, M.; Brodbelt, J. S. *Anal. Chem*. **2000**, *72*, 5898.
(13) Shvartsburg, A. A.; Jones, R. C. *J. Am. Soc. Mass Spectrom.* **2004**, *15*, 406.
(14) Harvey, J. N.; Kaczorowska, M. *Int. J. Mass Spectrom*. **2003**, *228*, 517.
(15) Hughes, S. R.; Nguyen, T. N.; Capobianco, J. A.; Peslherbe, G. H. *Int. J. Mass Spectrom.* **2005**, *241*, 283.
(16) Xiao, C.; Hagelberg, F.; El-Nahas, A. M. *J. Phys. Chem. A* **2004**, *108*, 5322.
(17) Shi, T. J.; Zhao, J. F.; Hopkinson, A. C; Siu, K. W. M. *J. Phys. Chem. B* **2005**, *109*, 10590.
(18) Jacob, A. P.; James, P. F; O'Hair, R. A. J. *Int. J. Mass Spectrom*. **2006**, *255*, 45.
(19) Wright, R. R.; Walker, N. R.; Firth, S.; Stace, A. J. *J. Phys. Chem. A* **2001**, *105*, 54.
(20) Spears, K. G.; Fehsenfeld, F. C. *J. Chem. Phys.* **1972**, *56*, 5698.
(21) Jayaweera, P.; Blades, A. T.; Ikonomou, M. G.; Kebarle, P. *J. Am. Chem. Soc.* **1990**, *112*, 2452.
(22) Cheng, Z. L; Siu, K. W. M.; Guevremont, R.; Berman, S. S. *J. Am. Soc. Mass Spectrom*. **1992**, *3*, 281.
(23) Dobson, M. P.; Stace, A. J. *Chem. Commun*. **1996**, 1533.
(24) Stace, A. J. *J. Phys. Chem. A* **2002**, *106*, 7993.
(25) Schröder, D.; Schwarz, H. *J. Phys. Chem. A* **1999**, *103*, 7385.
(26) Schröder, D.; Schwarz, H.; Wu, J.; Wesdemiotis, C. *Chem. Phys. Lett.* **2001**, *343*, 258.
(27) Puskar, L.; Barran, P. E.; Duncombe, B. J.; Chapman, D.; Stace, A. J. *J. Phys. Chem. A* **2005**, *109*, 273.
(28) Walker, N. R.; Wright, R. R.; Barran, P. E.; Cox, H.; Stace, A. J. *J. Chem. Phys.* **2001**, *114*, 5562.
(29) Shi, T.; Orlova, G.; Guo, J.; Bohme, D. K.; Hopkinson, A. C.; Siu, K. W. M. *J. Am. Chem. Soc*. **2004**, *126*, 7975.
(30) Kohler, M.; Leary, J. A. *J. Am. Soc. Mass Spectrom.* **1997**, *8*, 1124.
(31) Kohler, M.; Leary, J. A. *Int. J. Mass Spectrom.* **1997**, *162*, 17.
(32) Shvartsburg, A. A.; Wilkes, J. G.; Lay, J. O.; Siu, K. W. M. *Chem. Phys. Lett*. **2001**, *350*, 216.
(33) Shvartsburg, A. A.; Wilkes, J. G. *J. Phys. Chem. A* **2002**, *106*, 4543.
(34) Stone, J. A.; Su, T.; Vukomanovic, D. *Can. J. Chem.* **2005**, *83*, 1921.
(35) Shvartsburg, A. A. *Chem. Phys. Lett*. **2003**, *376*, 6.
(36) Akibo-Betts, G.; Barran, P. E.; Stace, A. J. *Chem. Phys. Lett*. **2000**, *329*, 431.
(37) Shvartsburg, A. A.; Siu, K. W. M. *J. Am. Chem. Soc*. **2001**, *123*, 10071.
(38) Shvartsburg, A. A.; Wilkes, J. G. *Int. J. Mass Spectrom*. **2003**, *225*, 155.
(39) Shvartsburg, A. A. *J. Am. Chem. Soc.* **2002**, *124*, 12343.
(40) Bush, M. F.; Saykally, R. J.; Williams, E. R. *Int. J. Mass Spectrom.* **2006**, *253*, 256.
(41) El-Nahas, A. M.; Tajima, N.; Hirao, K. *Chem. Phys. Lett*. **2000**, *318*, 333.
(42) Stone, J. A.; Vukomanovic, D. *Chem. Phys. Lett.* **2001**, *346*, 419.
(43) El-Nahas, A. M. *Chem. Phys. Lett.* **2002**, *365*, 251.
(44) Stone, J. A.; Su, T.; Vukomanovic, D. *Int. J. Mass Spectrom.* **2002**, *216*, 219.
(45) Xiao, C.; Walker, K.; Hagelberg, F.; El-Nahas, A. M. *Int. J. Mass Spectrom.* **2004**, *233*, 87.
(46) Cheng, Z. L.; Siu, K. W. M.; Guevremont, R.; Berman, S. S. *Org. Mass Spectrom.* **1992**, *27*, 1370.
(47) Walker, N.; Dobson, M. P.; Wright, R. R.; Barran, P. E.; Murrell, J. N.; Stace, A. J. *J. Am. Chem. Soc.* **2000**, *122*, 11138.
(48) Duncombe, B. J.; Puskar, L.; Wu, B. H.; Stace, A. J. *Can. J. Chem.* **2005**, *83*, 1994.
(49) Puskar, L.; Stace, A. J. *Mol. Phys.* **2005**, *103*, 1829.
(50) Frisch, M. J. et al. *Gaussian 03*, revision C.02; Gaussian, Inc.: Wallingford, CT, 2004.
(51) Kresse, G.; Hafner, J. *Phys. Rev. B* **1993**, *47*, 558.
(52) Kresse, G.; Hafner, J. *Phys. Rev. B* **1994**, *49*, 14251.
(53) Kresse, G.; Furthmüller, J. *Comp. Mater. Sci.* **1996**, *6*, 15.
(54) Kohn, W.; Sham, L. J. *Phys. Rev.* **1965**, *140*, A1133.
(55) Wood, D. M.; Zunger, A. *J. Phys. A* **1985**, *18*, 1343.
(56) Pulay, P. *Chem. Phys. Lett.* **1980**, *73*, 393.
(57) Bloechl, P. E. *Phys. Rev. B* **1994**, *50*, 17953.
(58) Perdew, J. P.; Wang, Y. *Phys. Rev. B* **1992**, *45*, 13244.
(59) Shi, T.; Siu, K. W. M.; Hopkinson, A. C. *Int. J. Mass Spectrom.* **2006**, *255*−*256*, 251.
(60) Chesnavich, W. J.; Bass, L.; Su, T.; Bowers, M. T. *J. Chem. Phys.* **1981**, *74*, 2228.
(61) Stace, A. J.; Walker, N. R.; Wright, R. R.; Firth, S. *Chem. Phys. Lett.* **2000**, *329*, 173.
(62) Stone, J. A.; Vukomanovic, D. *Int. J. Mass Spectrom.* **1999**, *185/186/187*, 227.
(63) Rodgers, M. T.; Armentrout, P. B. *Acc. Chem. Res.* **2004**, *37*, 989.